THE JOURNAL OF BIOLOGICAL CHEMISTRY VOL. 280, NO. 50, pp. 41482–41486, December 16, 2005

The Structure of Human SULT1A1 Crystallized with Estradiol

*AN INSIGHT INTO ACTIVE SITE PLASTICITY AND SUBSTRATE INHIBITION WITH MULTI-RING SUBSTRATES**

Received for publication, July 28, 2005, and in revised form, October 7, 2005 Published, JBC Papers in Press, October 12, 2005, DOI 10.1074/jbc.M508289200

Niranjali U. Gamage[‡], Sergey Tsvetanov[§], Ronald G. Duggleby[§], Michael E. McManus[‡], and Jennifer L. Martin[¶1]

From the [‡]School of Biomedical Sciences, [§]School of Molecular and Microbial Sciences, and [¶]Institute for Molecular Bioscience, University of Queensland, Brisbane, Queensland 4072, Australia

Human SULT1A1 belongs to the supergene family of sulfotransferases (SULTs) involved in the sulfonation of xeno- and endobiotics. The enzyme is also one of the SULTs responsible for metabolic activation of mutagenic and carcinogenic compounds and therefore is implicated in various cancer forms. Further, it is not well understood how substrate inhibition takes place with rigid fused multi-ring substrates such as 17β-estradiol (E2) at high substrate concentrations when subcellular fractions or recombinant enzymes are used. To investigate how estradiol binds to SULT1A1, we co-crystallized SULT1A1 with sulfated estradiol and the cofactor product, PAP (3′-phosphoadenosine 5′-phosphate). The crystal structure of SULT1A1 that we present here has PAP and one molecule of E2 bound in a nonproductive mode in the active site. The structure reveals how the SULT1A1 binding site undergoes conformational changes to accept fused ring substrates such as steroids. In agreement with previous reports, the enzyme shows partial substrate inhibition at high concentrations of E2. A model to explain these kinetics is developed based on the formation of an enzyme·PAP·E2 dead-end complex during catalysis. This model provides a very good quantitative description of the rate *versus* the [E2] curve. This dead-end complex is proposed to be that described by the observed structure, where E2 is bound in a nonproductive mode.

Cytosolic sulfotransferases (SULTs)[2] are involved in the phase II metabolism of numerous xeno- and endobiotics such as drugs, neurotransmitters, bile acids, and hormones (1, 2). SULTs utilize the cofactor 3′-phosphoadenosine 5′-phosphosulfate (PAPS) as the sulfonate (SO_3^{-1}) donor in such reactions that generally lead to the detoxification of substrates by making them more water-soluble and thereby readily excretable via the kidneys. However, in the case of mutagenic and carcinogenic *N*-hydroxyarylamines and heterocyclic amines and benzylic alcohols of polycyclic aromatic hydrocarbons, sulfonation is a critical step in their metabolic activation to electrophiles that can bind tissue macromolecules such as DNA (3–6). Further, sulfonation has been shown to activate the antihypertensive and hair growth stimulant minoxidil (7). The overall role that sulfonation plays in disease states such as neurodegeneration and cancer is currently under active investigation (8–10).

SULT1A1 has a broad tissue distribution and has been shown to metabolize a wide range of xenobiotics and play a significant role in the metabolism of estrogens and iodothyronines. In resolving the crystal structure (11) of SULT1A1 we showed that it contains a very hydrophobic L-shaped substrate-binding region, which explains how it can accommodate small planar compounds as well as larger L-shaped aromatics such as iodothyronines. However, in those studies we could not explain how extended fused ring systems, such as 17β-estradiol (E2), can act as substrates of SULT1A1. In addition, no real information has been provided as to why the metabolism of E2 is inhibited at high concentrations of substrate when subcellular fractions or recombinant enzymes are employed as the catalytic sources.

Recent studies from our laboratory on the crystal structure of SULT1A1 gave the first insight into understanding how substrate inhibition takes place with small planar substrates such as *p*-nitrophenol (*p*NP). In that study we showed that the active site of SULT1A1 is capable of binding two molecules of *p*NP simultaneously (11). Further, we have demonstrated, using both molecular modeling and site-directed mutagenesis, that SULT1A3 can bind two molecules of dopamine in its active site (12). From these studies we have been able to conclude that substrate inhibition at high concentrations is caused by impeded catalysis when both binding sites are occupied. In the present study, we have determined the crystal structure of the SULT1A1·PAP·E2 complex. The results demonstrate how the enzyme adapts its substrate binding site to enable binding of the fused steroid ring system, supporting the notion of active site plasticity. The structure also reveals that E2 interacts in a nonproductive manner when co-crystallized with PAP. The relationship of this binding mode to the phenomenon of substrate inhibition that has been observed with E2 was investigated, and a general model of substrate inhibition, relevant to all SULTs with any substrate bound, has been proposed.

EXPERIMENTAL PROCEDURES

Protein Expression and Purification—Human SULT1A1 cDNA was expressed in *Escherichia coli* as an N-terminal hexahistidine fusion protein, using a pET-28a(+) vector as described previously (13–15). The protein was purified by TALON cobalt affinity resin (Clontech) and gel filtration chromatography and then concentrated to 20 mg ml^{-1} in 20 mM Tris (pH 8.0) and 10 mM dithiothreitol. The purity of the protein was assessed using SDS-PAGE.

Crystallization—Crystallization of SULT1A1 was carried out by the hanging drop vapor diffusion method. Initial conditions were identified using commercial (Hampton Research) and polyethylene glycol screens and optimized by incremental scanning around initial conditions. The optimized conditions for crystallization were as follows. Purified

* This work was supported by Grant 252734 from the National Health and Medical Research Council of Australia. The costs of publication of this article were defrayed in part by the payment of page charges. This article must therefore be hereby marked "*advertisement*" in accordance with 18 U.S.C. Section 1734 solely to indicate this fact.
The atomic coordinates and structure factors (code 2D06) have been deposited in the Protein Data Bank, Research Collaboratory for Structural Bioinformatics, Rutgers University, New Brunswick, NJ (http://www.rcsb.org/).
[1] To whom correspondence should be addressed: Inst. for Molecular Bioscience, University of Queensland, Brisbane, Queensland 4072, Australia. Tel.: 61-7-3365-4942; Fax: 61-7-3365-1990; E-mail: j.martin@imb.uq.edu.au.
[2] The abbreviations used are: SULT, sulfotransferase; PAP, 3′-phosphoadenosine 5′-phosphate; PAPS, 3′-phosphoadenosine 5′-phosphosulfate; *p*NP, *p*-nitrophenol; E2, 17β-estradiol; E2S, sulfonated estradiol; DHEA, dehydroepiandrosterone; DHEA-ST, dehydroepiandrosterone sulfotransferase.

TABLE ONE

Data collection and refinement statistics

Values in parentheses refer to the highest resolution shell (2.30–2.38 Å). r.m.s.d., root mean square deviation.

Data Collection	
Unit cell	
a (Å)	123.6
b (Å)	86.1
c (Å)	73.0
α, β, γ (degree)	90
Space group	$P2_12_12$
Molecules in asymmetric unit	2
Observations[a]	105,909
Unique reflections[a]	35,207
R_{sym} (%)[b]	9.4 (44.2)
$I/\sigma I$	6.1 (2.2)
Completeness (%)	99.5 (99.8)
Refinement	
R-factor[c]	22.7% (47.6%)
R-free[c]	28.3% (46.1%)
No. of water molecules	120
Average B-factor (Å^2)	45
Resolution range (Å)	31–2.3
r.m.s.d. from ideal	
Bond lengths (Å)	0.012
Bond angles (degree)	1.614
Ramachandran statistics	
Residues in most favored region (%)	90.0
Residues in additionally allowed region (%)	10.0
Residues in disallowed regions (%)	0

[a] No sigma cutoff was applied to these data, but a total of 801 of 106,710 observations (0.75%) was rejected based on the criteria that any observation for which *I* deviates by >5.98 σI from the average *I* for that reflection is rejected.

[b] $R_{sym} = \Sigma|I - \langle I\rangle|/\Sigma(I)$.

[c] *R*-factor = $\Sigma||F_o| - |F_c||/\Sigma|F_o|$ (F_o and F_c are the observed and calculated structure factors respectively). *R*-free is calculated from 10% of the data that have been excluded from refinement. Reflections were rejected during refinement where $|F|/\sigma F < 0$. A total of 35,123 reflections was used in refinement (31,615 for *R*-factor and 3,508 for *R*-free calculation).

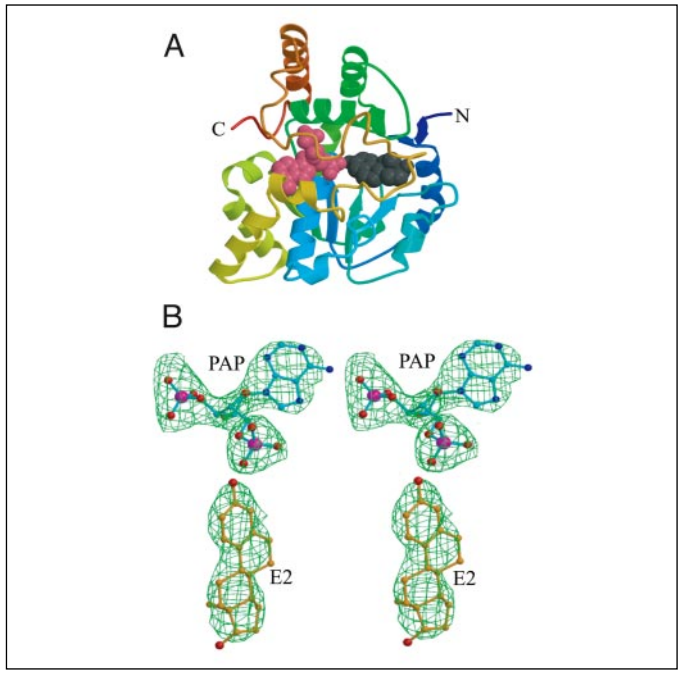

FIGURE 1. *A*, crystal structure of human SULT1A1 complexed with E2 and PAP. The Cα trace is colored *blue* (N terminus) to *red* (C terminus). Secondary structural elements are represented by *coils* for helices and *arrows* for strands. The bound ligands are shown as *space-filled models*: *pink*, PAP; *dark gray*, E2. *B*, stereoview of simulated annealed $F_o - F_c$ omit maps (contoured at 3.0 σ; ligands excluded from the calculation) at the active site of SULT1A1 showing the binding of PAP and E2. Atom coloring: *dark blue*, nitrogen; *red*, oxygen; *purple*, phosphorus; *light blue*, PAP carbon; *orange*, E2 carbon.

SULT1A1 (20 mg ml^{-1}) was preincubated with 45 mM PAP and 5 mM estradiol or sulfated estradiol (β-estradiol 3-sulfate sodium salt in 70% *N*-methyl-D-glucamine) on ice for at least 30 min. Then, 1 μl of the protein solution was mixed with 1 μl of the well solution (0.1 M Tris-HCL, pH 8.0, 20% polyethylene glycol 4000) on a coverslip, placed over the well solution, and equilibrated at 20 °C. Crystals (~0.3 × 0.2 × 0.2 mm) appeared 3–4 days after microseeding.

X-ray Diffraction Data Measurement—Data were measured on an R-AXIS IV^{++}/RU-200 x-ray generator with Osmic Blue mirror optics. Cryocooling was evaluated for data measurement. However, without added cryoprotectant the diffraction was weak and streaky. Increasing the polyethylene glycol concentration to 25% gave the same result. Dunking crystals into solutions containing cryoprotectant (glycerol) caused immediate crystal cracking, and stepwise soaking resulted in crystal cracking above 5% glycerol. Therefore, the diffraction data were measured at room temperature (17 °C); crystals were mounted in quartz capillary tubes, and diffraction data were measured to 2.3 Å resolution and processed with Crystal Clear© (Rigaku Corp.).

Structure Determination—The structure of SULT1A1 (Protein Data Bank code 1LS6) with ligands *p*NP and PAP removed was used as the search model for phasing by molecular replacement. The molecular replacement solution from CNS (crystallography and NMR system) (16) gave two molecules of SULT1A1 in the asymmetric unit. Rigid body refinement of this solution gave initial *R*-factor and *R*-free values of 34.2 and 34.9%, respectively. Simulated annealing by cartesian molecular dynamics followed by *B*-factor refinement improved these values to 26.9 and 31.8%, respectively. After several rounds of model building in O (17) and refinement in CNS, a final *R*-factor of 22.7% and an *R*-free value of 28.3% were obtained. Residues 8–295 were modeled for both SULT1A1 molecules in the asymmetric unit, and each molecule contains a bound PAP and E2. 120 water molecules were included (TABLE ONE), and alternate conformations were modeled for the side chains of Glu^{166}, Met^{260}, and Cys^{287}. Coordinates and structure factors have been deposited in the Protein Data Bank (18) with code 2D06.

SULT Activity Assay—Enzyme activity was measured according to the modified method of Foldes and Meek (19). The reaction mixture contained 10 mM phosphate buffer (pH 7.0), 20 μM [^{35}S]PAPS, 0.1 μg/ml SULT1A1, and varying concentrations of E2. E2 was dissolved in 100% ethanol, and the maximum ethanol concentration used in the reaction mixture was 1% to prevent inhibition of the enzyme by ethanol. The final volume of the reaction mix was 500 μl. Reactions were initiated by adding the enzyme to the reaction mixture and incubating this mixture for 20 min at 37 °C. The sulfonation reaction was terminated by adding 0.1 M barium acetate, barium hydroxide, and zinc sulfate. Incubation times and protein concentrations used were within the linear range for product formation with E2 as the substrate. Assays were performed in duplicate, and background activity was corrected using controls with no substrate added. Radioactivity of the sulfonated E2 was measured using a liquid scintillation counter (Tri-Carb 2500, Packard).

Molecular Modeling—To dock E2 in the catalytically productive mode, PAPS was modeled into the SULT1A1 structure based on the SULT1E1-PAPS structure (Protein Data Bank code 1HY3 (20)). E2 was docked using GOLD (21) with 10 genetic algorithm runs and default parameters. Figures were prepared using Molscript (22) and Raster 3d (23). Structural comparisons of SULT1A1, mouse SULT1E1 (24), and

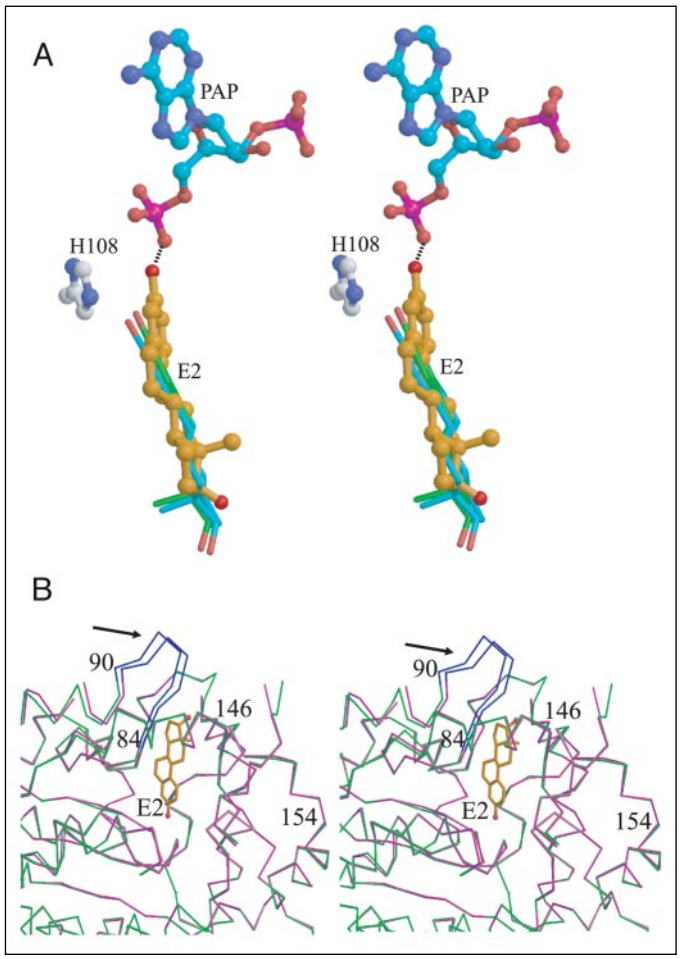

FIGURE 2. **Comparison of fused ring substrate binding in SULT1A1, mouse SULT1E1, and human SULT2A1.** *A*, stereoview of E2 binding in the SULT1A1 active site. The noncatalytic substrate binding mode of SULT1A1 is shown in *orange*. The O-3 hydroxyl of E2 can form hydrogen bonds (*dotted lines*) to PAP and Lys[48] (not shown for clarity). The proposed E2 catalytic orientation (*green*) was modeled using GOLD. For comparison, the E2 binding mode from mouse SULT1E1 is shown (*light blue*). *B*, superimposition of Cα traces of SULT1A1·PAP·*p*NP (*pink*) and SULT1A1·PAP·E2 (*green*). E2 is shown in *orange*. A loop (residues 84–90) that moves to accommodate E2 in the active site is highlighted in *dark blue* and indicated by an *arrow*.

DHEA-ST (25) were performed using the lsq options of O (17). DHEA-ST is referred to as SULT2A1, according to the new SULT nomenclature (26).

RESULTS

The crystal structure of the SULT1A1·PAP·E2 complex was solved to 2.3 Å resolution (Fig. 1). Crystals were orthorhombic (space group $P2_12_12$ with two molecules in the asymmetric unit). The overall structure is similar to that for SULT1A1·PAP·*p*NP (Protein Data Bank code 1LS6 (11)) with the core α/β domain found in all SULTs comprising a central five-stranded parallel β-sheet that forms the catalytic and PAPS binding sites (Fig. 1). The binding mode of the product, PAP, is similar to that described for the SULT1A1·PAP·*p*NP structure (11).

Substrate Binding Site—We first attempted to crystallize SULT1A1 with PAP and E2, but the bound conformation of E2 was not catalytically competent. Therefore, crystallization was repeated, replacing E2 with a saturating concentration of sulfonated E2 (E2S). However, E2 rather than E2S was again bound at the active site in a noncatalytic mode. NMR analysis of the sample revealed >90% E2S. This suggested that E2 is formed from E2S under the crystallization conditions. Could the enzyme catalyze the reverse reaction? Because E2S is a sulfate ester,

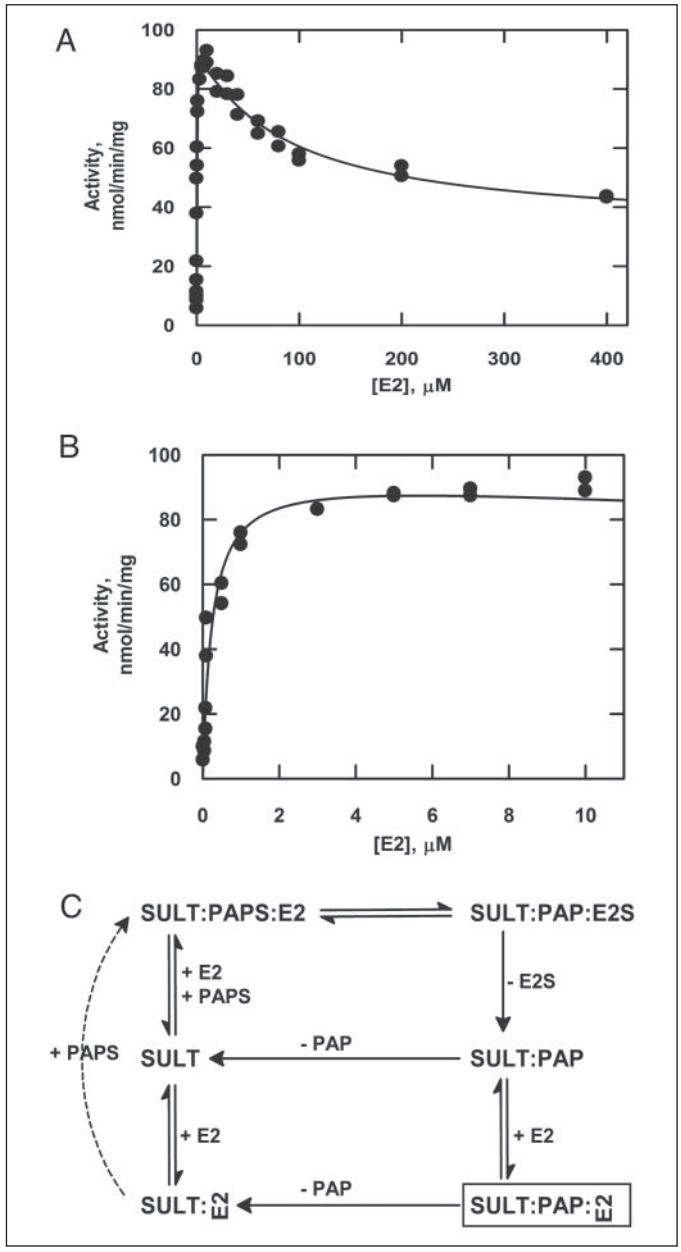

FIGURE 3. **Substrate inhibition of SULT1A1 by E2.** *A*, data obtained at E2 concentrations up to 400 μM. *B*, expanded view of the data in the low concentration range (up to 10 μM). *Lines* represent a best fit to the data of Equation 5, with $V_m = 94.9 \pm 2.9$ nmol/mg/min, $V_{lim} = 32.0 \pm 7.5$ nmol/mg/min, $K_m = 0.243 \pm 0.032$ μM, and $K_i = 83.2 \pm 32.0$ μM. Nonlinear regression was performed with the GraFit program (Erithacus Software, Horley, UK). *C*, kinetic model explaining the observed substrate inhibition. The enzyme binds the two substrates giving SULT·PAPS·E2 and then undergoes catalysis and release of the products E2S and PAP. Alternatively, the SULT·PAP complex can bind E2 in the nonproductive mode (indicated with E2 drawn sideways) giving a complex that can reenter the catalytic pathway by releasing PAP followed by E2. The rate equation (Equation 5) for this model was derived using the REFERASS program (33). The *broken line* shows an alternative model that allows PAPS binding to follow that of E2. The crystal structure reported in this paper is represented by the *boxed* complex.

whereas PAPS is an acid anhydride, thermodynamics would not favor the reverse reaction. However, a reasonable $\Delta G^{o\prime}$ of 15.5 kJ/mol under the conditions employed would allow formation of ~0.6 mM E2, equal to the enzyme concentration used for crystallization. If E2 binds to the enzyme in preference to E2S, this would account for the formation of the observed complex. In addition, if the PAPS formed in this reverse reaction is hydrolyzed, it would push the equilibrium in this direction and thus increase the amount of E2 formed. Although PAPS is fairly

stable, an accelerated breakdown by aminolysis might be expected (27) during crystallization, which in our experiment required incubation for several days in Tris buffer.

The O-3 hydroxyl of E2 is the target for sulfonation by SULT1A1, but in the noncatalytic binding mode reported here, the O-3 atom is located very close to the cofactor product, PAP. In this mode, there is no room to model a sulfonate onto either PAP or E2. The E2 hydroxyl forms hydrogen bonds to the PAP phosphate (2.6 Å, Fig. 2*A*) and to the backbone nitrogen of Lys[48] (3.2 Å, not shown). The superimposition of noncatalytic E2 with modeled E2 in a catalytically competent binding mode and with E2 from the SULT1E1 structure (24) is also shown (Fig. 2*A*). E2 is shifted ~2 Å toward PAP in the noncatalytic mode compared with the catalytic binding mode. The docked E2 has a binding mode similar to that observed in the SULT1E1 crystal structure (both are 2.9–3.0 Å from the catalytic His[108]). The binding pocket for E2 is well ordered in the SULT1A1 structure, and the substrate is surrounded by hydrophobic residues. As in the SULT1A1·PAP·*p*NP structure, Phe[142] and Phe[81] form a substrate access gate that permits binding of planar substrates.

Kinetics of E2 Sulfonation by SULT1A1—SULT1A1 shows strong substrate inhibition by E2 (Fig. 3, *A* and *B*). The inhibition at high E2 concentrations can be explained in the following manner. For E2 to behave both as a substrate and a competitive inhibitor, binding in the productive and nonproductive orientations must be mutually exclusive. Using the standard equation for competitive inhibition, we get

$$v = V_m[\mathrm{E2}]/\{K_m(1 + [\mathrm{E2}]/K_i) + [\mathrm{E2}]\} \qquad \text{(Eq. 1)}$$

where V_m is the maximum rate, K_m is the Michaelis constant for E2, and K_i is the inhibition constant for E2. This can be simplified to

$$v = V_m{}^{\mathrm{app}}[\mathrm{E2}]/\{K_m{}^{\mathrm{app}} + [\mathrm{E2}]\} \qquad \text{(Eq. 2)}$$

where,

$$V_m{}^{\mathrm{app}} = V_m/(1 + K_m/K_i) \qquad \text{(Eq. 3)}$$

$$K_m{}^{\mathrm{app}} = K_m/(1 + K_m/K_i) \qquad \text{(Eq. 4)}$$

Thus, Michaelis-Menten kinetics will be followed in this situation, and substrate misorientation will be undetectable from the substrate saturation curve.

The formation by SULTs of dead-end complexes, containing one of the substrates and one of the products, has been discussed previously (28–30). The existence of such complexes has been deduced from kinetic experiments, and the complex that is crystallized here is a direct demonstration of its existence. If this SULT·PAP·E2 complex forms during catalysis, it provides a ready explanation for substrate inhibition as depicted in the proposed mechanism (Fig. 3*C*). After substrate binding and catalysis, the SULT·PAP·E2S complex releases E2S. The SULT·PAP complex can then release PAP, to complete the catalytic cycle, or bind E2 in the nonproductive mode. The formation of this complex would be favored at high E2 concentration, resulting in substrate inhibition. However, we observed (Fig. 3, *A* and *B*) that substrate inhibition was incomplete, which suggests that this complex can reenter the catalytic pathway by release of PAP followed by release of E2.

The rate equation for this situation (at saturating [PAPS]) is

$$v = \{V_m[\mathrm{E2}] + V_{\mathrm{lim}}[\mathrm{E2}]^2/K_i\}/\{K_m + [\mathrm{E2}] + [\mathrm{E2}]^2/K_i\} \qquad \text{(Eq. 5)}$$

where V_m, K_m, and K_i are as described for Equation 1 and V_{lim} is the limiting rate at high [E2]. Fitting this equation to the data gives the kinetic constants shown in the legend to Fig. 3. There is excellent agreement between Equation 5 and the experimental data.

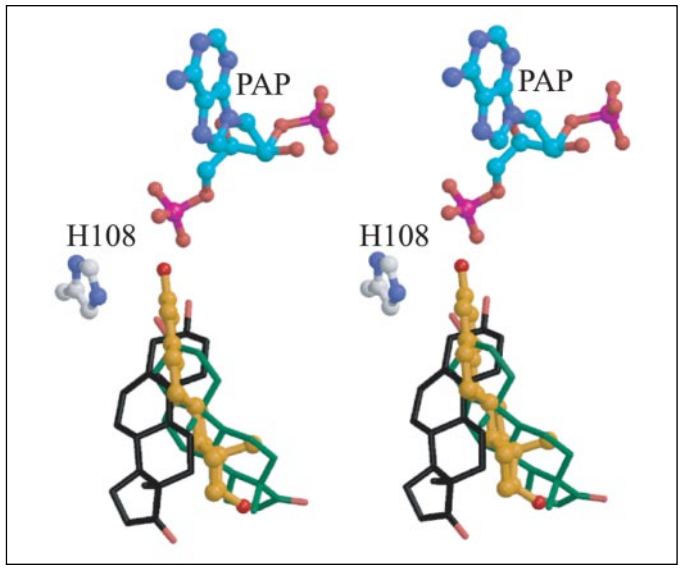

FIGURE 4. **Stereoview comparing the binding modes of E2 (*orange*) bound to SULT1A1 and DHEA bound to SULT2A1.** The productive or catalytic orientation of DHEA is shown in *green*, and the nonproductive orientation is in *black*. PAP (*light blue*) and the catalytic His[108] (*gray*) of SULT1A1 are shown in a *ball-and-stick* representation.

It is of interest that the misoriented E2 is not a necessary feature of the model. If E2 was correctly oriented the SULT·E2 complex could move directly back into catalysis by binding PAPS to form SULT·PAPS·E2. In Fig. 3*C*, this corresponds to the reaction shown by the *broken line*. The rate equation for this alternative model is the same as Equation 5.

We emphasize that the structure we have determined containing one of the substrates (E2) and one of the products (PAP) (Fig. 2*A*) is a dead-end complex rather than an intermediate on the normal catalytic pathway. Formation of this complex during catalysis, by binding of the substrate E2 before PAP is released, is the reason that there is substrate inhibition. The misorientation of E2 in this complex is a secondary consequence arising because neither E2 nor PAP has a sulfonate group. This allows E2 to penetrate further into the active site and to form hydrogen bonds to PAP and the backbone of Lys[48]. Substrate inhibition results because the dead-end complex can form and would still be expected even if E2 was oriented correctly.

DISCUSSION

Human SULT1A1 is involved in detoxification and bioactivation of a broad range of substrates including iodothyronines, hydroxyaryl amines, estrogens, and phenolic xenobiotics. These substrates can be small planar aromatics (phenols), large L-shaped aromatics (iodothyronines), or extended planar aromatic ring systems (estrogen, hydroxylamines, and heterocyclic hydroxylamines). The crystal structure of SULT1A1 and modeling studies have shown how small planar molecules such as *p*NP and L-shaped aromatics (iodothyronines) can bind to the active site (11) but have not explained how extended multi-ring systems such as E2 interact with the enzyme. We proposed that the SULT1A1 active site is plastic and adopts various shapes to accept different types of molecules (11). Previously, we reported an L-shaped binding site in the structure when SULT1A1 was crystallized with *p*NP (11). However, E2 has a fused ring system that cannot adopt an L-shaped conformation. Instead, a conformational change in the binding site of the enzyme extends the accessible surface to allow binding of the

fused ring substrate. Two loop regions that close tightly over the SULT1A1·*p*NP complex are opened up in the present structure (Fig. 2*B*, residues 146–154 between α6 and α7, and particularly residues 84–90 just preceding α4), increasing the space available for E2 binding.

Another flexible region is the loop that connects α12 and α13 in SULT1A1; this loop covers the substrate upon binding and is involved in several direct contacts with bound E2. Phe^{247} is located in this loop and appears to play an important role in E2 binding in SULT1A1. When 3,3′-diiodothyronine (T2) was modeled into the SULT1A1 structure, a catalytically competent binding mode was possible only if Phe^{247} adopted an alternate rotamer conformation (11). We showed, using molecular modeling and site-directed mutagenesis, that this residue also plays an important role in substrate inhibition of SULT1A1 (12). In the present structure we observed that Phe^{247} does indeed adopt a conformation different from that in the SULT1A1·*p*NP crystal structure, thereby increasing the space available to bind the fused ring structure of the steroid.

A characteristic feature of SULTs is substrate inhibition at high concentrations of their preferred substrates (31, 32). We have proposed a kinetic model for *p*NP substrate inhibition in SULT1A1 based on the crystallographic evidence of two *p*NP molecules in the active site (11). In that structure, one *p*NP molecule is in the correct position for sulfonation, whereas the second *p*NP molecule blocks the channel that leads to the active site. This suggests impeded catalysis when both binding sites are occupied. When only the second *p*NP is bound, access to the catalytic residues is likely be blocked. We proposed that it is the combination of these two events that gives rise to the substrate inhibition in SULT1A1 with *p*NP.

The crystal structure of SULT2A1 revealed that the substrate steroid DHEA can bind in either a productive or nonproductive mode (25). In the productive or catalytic orientation, DHEA has the O-3 hydroxyl positioned correctly for catalysis with respect to His^{99} and a modeled PAP. The alternative orientation places O-3 2.9 Å away and closer to the modeled PAP. The two binding modes overlap so that, in the absence of PAPS, the binding of DHEA in the productive and nonproductive modes must be mutually exclusive; only one DHEA molecule can be present in the active site at any given time, and it is likely that the ligand can adopt each orientation with similar probability. Rehse *et al.* (25) suggested that the alternative binding orientation could be the source of substrate inhibition in this enzyme, but our analysis (Equations 2–4) shows that this would not result in substrate inhibition (characterized by a decreasing rate with increasing substrate concentration, compare Equations 2–4 with Equation 5). As the substrate concentration increases, the amounts of productive and nonproductive modes would increase in the same proportion to one another, whereas substrate inhibition would require a relative increase in the proportion of the nonproductive mode.

We observed a nonproductive substrate orientation for E2 in SULT1A1, resembling the orientation for DHEA in SULT2A1, except that there is also a 45° rotation of the DHEA steroid with respect to the catalytic orientation (Fig. 4). Our explanation for substrate inhibition is that E2 binds to the SULT1A1·PAP complex after catalysis and release of E2S (Fig. 3). The resulting complex is the one that we have crystallized, providing clear evidence that such an entity exists. This complex is capable of releasing PAP but more slowly than it would be released without bound E2. However, in the presence of PAPS, SULT1A1 binds E2 in a catalytically competent mode that allows transfer of sulfonate from the cofactor to E2, as shown in Fig. 2*A*. This model explains the observed partial substrate inhibition of SULT1A1 by E2 and provides a more general explanation for the substrate inhibition that appears to be a common feature of SULTs.

REFERENCES

1. Falany, C. N. (1997) *FASEB J.* **11,** 1–2
2. Jakoby, W. B, and Ziegler D. M. (1990) *J. Biol. Chem.* **265,** 20715–20718
3. Banoglu, E. (2000) *Curr. Drug. Metab.* **1,** 1–30
4. Chou, H. C., Lang, N. P., and Kadlubar, F. F. (1995) *Cancer Res.* **55,** 525–529
5. Glatt. H. R. (1997) *FASEB J.* **11,** 314–321
6. Glatt, H. (2000) *Chem. Biol. Interact.* **129,** 141–170
7. Meisheri, K. D., Johnson, G. A., and Puddington, L. (1993) *Biochem. Pharmacol.* **45,** 271–279
8. Wang, Y., Spitz, M. R., Tsou, A. M., Zhang, K., Makan, N., and Wu, X. (2002) *Lung Cancer* **35,** 137–142
9. Seth, P., Lunetta, K. L., Bell, D. W., Gray, H., Nasser, S. M., Rhei, E., Kaelin, C. M., Iglehart, D. J., Marks, J. R., Garber, J. E., Haber, D. A., and Polyak, K. (2000) *Cancer Res.* **60,** 6859–6863
10. Pasqualini, J. R. (2004) *Biochim. Biophys. Acta* **1654,** 123–143
11. Gamage, N. U., Duggleby, R. G., Barnett, A. C., Tresillian, M., Latham, C. F., Liyou, N. E., McManus, M. E., and Martin, J. L. (2003) *J. Biol. Chem.* **278,** 7655–7662
12. Barnett, A. C., Tsvetanov, S., Gamage, N. U., Martin, J. L., Duggleby, R. G., McManus, M. E. (2004) *J. Biol. Chem.* **279,** 18799–18805
13. Brix, L. A., Duggleby, R. G., Gaedigk, A., and McManus, M. E. (1999) *Biochem. J.* **337,** 337–343
14. Bidwell, L. M., McManus, M. E., Gaedigk, A., Kakuta, Y., Negishi, M., Pedersen, L., and Martin, J. L. (1999) *J. Mol. Biol.* **293,** 521–530
15. Gaedigk, A., Lekas, P., Berchuck, M., and Grant, D. M. (1998) *Chem. Biol. Interact.* **109,** 43–52
16. Brunger, A. T., Adams, P. D., Clore, G. M., Delano, W. L., Gros, P. Grosse-Kunstleve, R. W., Jiang, R. W., Kuszewski, J., Nilges, M., Pannu, N. S., Read, R. J., Rice, L. M., Simonson, T., and Warren, G. L. (1998) *Acta Crystallogr. Sect. D Biol. Crystallogr.* **54,** 905–921
17. Jones, T. A., Zou, J. Y., Cowan, S. W., and Kjelgaard, M. (1991) *Acta Crystallogr. Sect. A* **47,** 110–119
18. Berman, H. M., Westbrook, J., Feng, Z., Gilliland, G., Bhat, T. N., Weissig, H., Shindyaloy, I. N., and Bourne, P. E. (2000) *Nucleic Acids Res.* **28,** 235–242
19. Foldes, A., and Meek, J. L. (1973) *Biochim. Biophys. Acta* **327,** 365–374
20. Pedersen, L. C., Petrotchenko, E., Shevtsov, S., and Negishi, M. (2002) *J. Biol. Chem.* **277,** 17928–17932
21. Jones, G., Willett, P., Glen, R. C., Leach, A. R., and Taylor, R. (1997) *J. Mol. Biol.* **267,** 727–748
22. Kraulis, P. J. (1991) *J. Appl. Crystallogr.* **24,** 940–950
23. Merritt, E. A., and Bacon, D. (1997) *Methods Enzymol.* **277,** 505–524
24. Kakuta, Y., Pedersen, L. G., Carter, C. W., Negishi, M and Pedersen, L. C. (1997) *Nat. Struct. Biol.* **4,** 904–908
25. Rehse, P. H., Zhou, M., and Lin, S. X. (2002) *Biochem. J.* **364,** 165–171
26. Blanchard, R. L., Freimuth, R. R., Buck, J., Weinshilboum, R. M., Coughtrie, M. W. H. (2004) *Pharmacogenetics* **14,** 199–211
27. Bedford, C. T., Kirby, A. J., Logan, C. J., and Drummond, J. N. (1995) *Bioorg. Med. Chem.* **3,** 167–172
28. Duffel, M. W., and Jakoby, W. B. (1981) *J. Biol. Chem.* **256,** 11123–11127
29. Yang, Y.-S., Tsai, S.-W., and Lin, E.-S. (1998) *Chem. Biol. Interact.* **109,** 129–135
30. Marshall, A. D., McPhie, P., and Jakoby, W. B. (2000) *Arch. Biochem. Biophys.* **382,** 95–104
31. Raftogianis, R. B., Wood, T. C., and Weinshilboum, R. M. (1999) *Biochem. Pharmacol.* **58,** 605–616
32. Reiter, C., Mwaluko, G., Dunnette, J., Van Loon, J., and Weinshilboum, R. (1983) *Naunyn-Schmiedeberg's Arch. Pharmacol.* **324,** 140–147
33. Varón, R., García-Sevilla, F., García-Moreno, M., García-Cánovas, F., Peyró, R., and Duggleby, R. G. (1997) *Comput. Appl. Biosci.* **13,** 159–167